Environmental Science & Technology

pubs.acs.org/est

Article

Surveying Manganese Oxides as Electrode Materials for Harnessing Salinity Gradient Energy

Jenelle Fortunato, Jasquelin Peña, Sassi Benkaddour, Huichun Zhang, Jianzhi Huang, Mengqiang Zhu, Bruce E. Logan, and Christopher A. Gorski*

Cite This: *Environ. Sci. Technol.* 2020, 54, 5746−5754

Read Online

ACCESS | Metrics & More | Article Recommendations | Supporting Information

ABSTRACT: The potential energy contained in the controlled mixing of waters with different salt concentrations (i.e., salinity gradient energy) can theoretically provide a substantial fraction of the global electrical demand. One method for generating electricity from salinity gradients is to use electrode-based reactions in electrochemical cells. Here, we examined the relationship between the electrical power densities generated from synthetic NaCl solutions and the crystal structures and morphologies of manganese oxides, which undergo redox reactions coupled to sodium ion uptake and release. Our aim was to make progress toward developing rational frameworks for selecting electrode materials used to harvest salinity gradient energy. We synthesized 12 manganese oxides having different crystal structures and particle sizes and measured the power densities they produced in a concentration flow cell fed with 0.02 and 0.5 M NaCl solutions. Power production varied considerably among the oxides, ranging from no power produced (β-MnO_2) to 1.18 ± 0.01 W/m^2 (sodium manganese oxide). Power production correlated with the materials' specific capacities, suggesting that cyclic voltammetry may be a simple method to screen possible materials. The highest power densities were achieved with manganese oxides capable of intercalating sodium ions when their potentials were prepoised prior to power production.

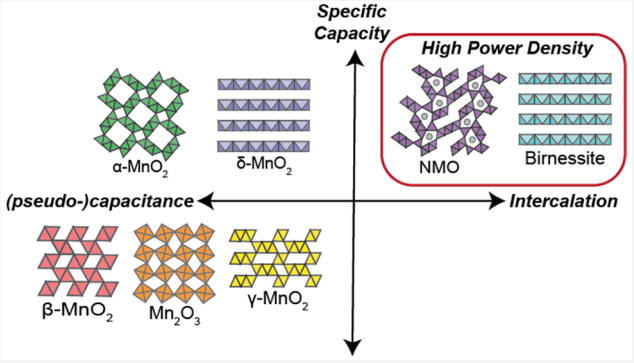

INTRODUCTION

The salt concentration difference between freshwater and seawater at coastlines is a largely unexploited yet abundant source of renewable energy.[1,2] The salinity gradient energy that can be obtained from mixing freshwater with seawater exceeds 0.8 kW·h/m^3 freshwater, which is roughly equivalent to freshwater flowing over a 250 m tall hydroelectric dam into the ocean.[3] It is estimated that the global amount of harvestable electricity from mixing freshwater with seawater is 8800 TW·h per year,[4] which is equal to 40% of the worldwide electricity production (21 600 TW·h in 2012).[5] Energy can also be obtained using more saline waters, such as hypersaline lakes and reject brines from desalination plants.[1−3] Currently, the two most extensively studied methods used to harvest salinity gradient energy are pressure retarded osmosis (PRO) and reverse electrodialysis (RED).[3−6] However, both technologies require selective membranes that either foul rapidly (PRO) or are prohibitively expensive (RED).[4,6,7] To overcome these membrane-related issues, researchers have begun studying electrochemical systems that harvest salinity gradient energy using electrode-based electrochemical reactions.[8−17]

The performances of salinity gradient energy technologies are usually compared in terms of electrical power densities (i.e., the rate of electricity production normalized to the area of a membrane or electrode).[2] While early electrode-based systems yielded low power densities (0.03−0.2 W/m^2)[9] relative to membrane-based systems (~1−10 W/m^2 for freshwater/seawater),[18] recent electrode-based studies have generated comparable values (3.3−3.8 W/m^2).[13,14] Achievable power densities have increased as a result of improved cell design, the introduction of a single ion exchange membrane to increase the cell voltage, and more effective electrode materials.[13,14,16] A major advance in electrode materials has derived from the transition from purely capacitive carbon-based electrode materials to electrode materials that charge via a combination of capacitive and faradaic mechanisms (e.g., Prussian Blue analogs and manganese oxides).[9,10,12−14] Materials that undergo faradaic reactions are often referred to as pseudocapacitive when the faradaic reaction rates are

Received: January 6, 2020
Revised: April 5, 2020
Accepted: April 6, 2020
Published: April 6, 2020

https://dx.doi.org/10.1021/acs.est.0c00096
Environ. Sci. Technol. 2020, 54, 5746−5754

sufficiently fast that they produce capacitor-like current−potential relationships.[19−22]

The promising electrical power densities produced by faradaic materials has led us to investigate how electrical power densities relate to a faradaic electrode material's electrochemical and physical properties. This work was motivated by the larger aim of developing frameworks for rationally selecting electrode materials to use in salinity gradient energy systems. We examined a suite of 12 manganese oxides having different crystal structures and/or particle sizes with respect to their electrochemical properties, physical properties, and electrical power densities produced from a NaCl salinity gradient. Manganese oxides are a useful model system because their syntheses can be adjusted to tune crystal structures, morphologies, and/or particle sizes[23−28] and because their charge storage mechanisms depend on their crystal structures. Manganese oxides may interact with Na^+ and Cl^- ions via capacitive or faradaic reactions that couple the reduction of Mn^{4+} to Mn^{3+} (or Mn^{3+} to Mn^{2+}) to the uptake of Na^+.[19,29,30] In this work, we refer to surface reactions that may involve capacitive or pseudocapacitive reactions as "(pseudo-)capacitive" because electrochemical techniques alone cannot distinguish between the two reactions. All 12 of the manganese oxides studied may undergo (pseudo)capacitive reactions at their surfaces, and a subset may also intercalate sodium ions (i.e., reversibly insert Na^+ into the crystal lattice without significantly altering the structure) into interlayer regions or tunnels (Figure 1).[21,22,24,25,27,31−34] We used cyclic voltammetry experiments conducted at several scan rates to assess the contribution of surface and intercalation reactions to power production and charge storage capacity. We then correlated power density data with characterization data to elucidate trends between power production and the physical and electrochemical properties of manganese oxides and thus identify which parameters might be indicative of material performance.

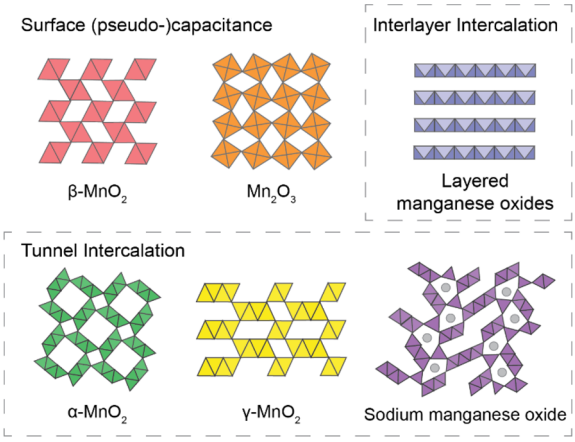

Figure 1. Representative crystal lattice structures and a hypothesized charge storage mechanism for the different manganese oxide crystal structures. All the manganese oxides exhibit some capacitive or pseudocapacitive surface charge storage. A portion of the materials are also hypothesized to intercalate sodium ions either in interlayers or in structural tunnels. The term layered manganese oxides refers to birnessite and δ-MnO_2. See Table S1 for tunnel and interlayer dimensions.

MATERIALS AND METHODS

All chemical reagents used in this study were analytical grade and were used without further purification. The deionized (DI) water used in syntheses and solutions had a resistivity of >18 MΩ·cm. The syntheses used to produce the 12 manganese oxides is provided in Section S1.

Inconsistencies exist in the literature regarding how manganese oxides are named.[23,26,35−37] Here, we classify the manganese oxides using the Greek prefix convention to allow us to differentiate among manganese oxides with different lattice arrangements of MnO_6 octahedral subunits. Tunneled manganese oxides were named on the basis of the size of the tunnel space: β-MnO_2 (1 × 1 tunnel), γ-MnO_2 (1 × 2 and 1 × 1 intergrowth), α-MnO_2 (2 × 2 tunnel) (Figure 1).[23,24] Layered manganese oxides were classified into two groups on the basis of crystallinity: birnessite and δ-MnO_2. We differentiated between the two on the basis of the X-ray diffraction patterns. Birnessites exhibit sharp X-ray diffraction peaks at 5.7° and 11.4° 2θ (Mo Kα; 7.28 and 3.64 Å) while δ-MnO_2 does not.[38] Note that one of the δ-MnO_2 specimens (δ-MnO_2-3) has been referred to as amorphous manganese oxide in the literature due to its poor crystallinity and broad X-ray powder diffraction peaks.[31,34] We classified this sample as δ-MnO_2 because the X-ray diffraction pattern and transmission electron microscopy images indicated the presence of short-range-ordered 2D-layer features, consistent with δ-MnO_2.

Material Characterization. Phase identification was performed using X-ray powder diffraction (XRD; Malvern PANalytical Empyrean X-ray diffractometer, 60.0 kV, 40.0 mA; molybdenum source: λ = 0.709 Å). All scans were performed in continuous scan mode within the 2θ range of 2.3078−30.5976°. A silicon standard was used to perform a background subtraction on all XRD patterns. Phase identification and background subtraction were performed in JADE for XRD software (Materials Data, Inc.). Field emission scanning electron microscopy (FESEM; FEI Verios G4 XHR SEM, ThermoFisher Scientific) was used to analyze sample morphology and particle size. Transmission electron microscopy (TEM; FEI Titan^3 G2 transmission electron microscope) was used to analyze crystal lattice structure. Cross-sections of manganese oxide samples for TEM analysis were prepared using ultramicrotomy. Powdered samples were prepared using a Spurr low-viscosity Embedding Kit (Sigma-Aldrich) and cured overnight at 60 °C. The cured resin was sectioned to 70 nm on a Leica Ultracut UC6 Ultramicrotome (Lecia Microsystems, Inc., Buffalo Grove, IL, USA). TEM imaging was performed using a spot size of 3, screen current of 0.5 nA, C2 aperture of 70 μm, and an exposure of 0.5 s with a binning of 2 s. The Brunauer−Emmett−Teller (BET) surface area was collected on each sample by analyzing 0.1 g of powder with a Micrometric ASAP 2020 Automated Surface Area and Porosimetry System using nitrogen gas and an analysis bath temperature of 77 K.

Electrode Preparation. Electrodes for each manganese oxide sample were prepared using a drop-cast fabrication method.[13,39] Electrodes were prepared by first heating 5 mL of *n*-methyl-2-pyrrolidinone (NMP) to dissolve 10 wt % (0.05 g) polyvinyldifluoride (PVDF) (Kynar HSV 900, Arkema, Inc.). Once cooled to room temperature, 70 wt % (0.35 g) manganese oxide powder and 20 wt % (0.1 g) carbon black (Vulcan XC72R, Cabot) were added and the mixture was thoroughly mixed. Using a pipet, 0.5 mL of the mixture was

https://dx.doi.org/10.1021/acs.est.0c00096
Environ. Sci. Technol. 2020, 54, 5746−5754

loaded onto precut carbon cloth (1071 HCB, AvCarb) and dried for 8 h in a vacuum oven at 55 °C, which removed the solvent.

Electrochemical Characterization. Electrochemical characterization tests were performed in a custom-built 3-electrode cell (Figure S1, volume ≈ 20 mL) with a CH Instruments 630e Potentiostat (Austin, TX).[13] The reactor was assembled with a titanium foil current collector, Ag/AgCl reference electrode (3 M KCl), and a platinum curly wire counter electrode. Cyclic voltammetry (CV) was used to measure the specific capacities of the manganese oxides. The specific capacities were measured as a function of scan rate (v = 0.1 to 50 mV/s) in 50 mM and 1 M NaCl solutions. All CVs began with a reductive sweep (0.8 to 0.2 V), followed by an oxidative sweep (0.2 to 0.8 V). Three scans were run at each scan rate to ensure material stability and equilibration. Specific capacities were calculated using the third scan by integrating the current and dividing by the manganese oxide mass in the electrode:

$$\text{specific capacity (F/g)} = \frac{\int_{T_1}^{T_2} I \, dt}{\Delta V \times m} \quad (1)$$

where I is current (C/s), which is integrated over time with respect to time, ΔV is the voltage window, and m is the mass of active electrode material.

To quantify the proportion of the current response that was due to (pseudo)capacitive reactions relative to intercalation reactions, we analyzed CVs for materials at several scan rates (v = 0.5, 1, 2, 5, and 10 mV/s). In a CV, the current response for a surface (pseudo)capacitive reaction scales directly with v, while the current response for a redox reaction limited by semi-infinite linear diffusion is proportional to $v^{1/2}$.[40] Past work has used this knowledge to quantify how much of the current is due to (pseudo)capacitive surface reactions ($I \propto v$) and intercalation reactions ($I \propto v^{1/2}$) by assuming that intercalation is a diffusion-controlled process.[22,41−43] Note the $I \propto v^{1/2}$ relationship is only valid for fully reversible diffusion-controlled reactions.[44] We used an established method for quantifying the relative contributions of these two processes:[22]

$$I_{peak} = av^b \quad (2)$$

where v is scan rate (mV/s), a and b are fitted parameters, and I_{peak} is the maximum current value achieved during the anodic or cathodic scan. The b value was calculated for each manganese oxide by taking the slope of $\log(I_{peak})$ vs $\log(v)$ during the anodic and cathodic sweeps and averaging the value. The reported b value for each manganese oxide is the average of these two values, with the error bars representing the cathodic and anodic values. A value of b = 1 indicates that the current is controlled entirely by surface (pseudo)capacitive reactions, while b = 0.5 indicates the current is controlled entirely by diffusion-controlled reactions, and an intermediate value indicates the relative contributions of both reactions to the overall current.[40]

Electrode Preconditioning. Electrodes were preconditioned to a desired potential immediately prior to performing each salinity gradient energy experiment. The as-prepared composite electrodes were conditioned in a 1 M NaCl solution in the custom-built 3-electrode setup described previously. Linear sweep voltammetry was performed at 1 mV/s, scanning from the measured open-circuit potential to the desired poise potential. Immediately following the linear sweep, electrodes were held at the poise potential until current was negligible (∼1 h). The electrodes were rinsed once in DI water and immediately placed in the concentration flow cell for testing.

Salinity Gradient Energy Experiments. Salinity gradient experiments were performed in a custom-built flow cell previously designed in our lab (Figure S2).[39] Graphite foil current collectors and manganese oxide electrodes were anchored at the two end plates. Spacer gaskets created rectangular flow paths (width = 1 cm; height = 3 cm; thickness ≈ 120 μm), and flow channels were separated by an anion exchange membrane (thickness ≈ 150 μm; Selemion AMV, Ashai Glass, Japan). High concentration (30 g/L, 0.5 M) and low concentration (1 g/L, 0.02 M) NaCl solutions were fed through the two channels at a flow rate of 15 mL/min. Power was generated and measured by connecting the electrode pair through an external resistor (R_{ext}), and the cell voltage (ΔE) was recorded using a potentiostat (VMP3, Bio-Logic). We measured the average power densities for each manganese oxide as a function of external resistance (5, 10, 20, 30, or 40 Ω). Power (W) at each time point was calculated by dividing the cell voltage by the applied external resistance ($P = \Delta E^2/R_{ext}$), and power density (W/m^2) was obtained by dividing by the projected electrode area (A = 2.94 cm^2). The average power density was calculated by averaging the power density over a complete discharge for three consecutive cycles, with the reported standard deviation representing the deviation between the cycles.

RESULTS AND DISCUSSION

Manganese Oxide Structures and Tunnel Dimensions. To determine how electrical power densities produced from sodium chloride-based salinity gradients depended on the manganese oxide in the electrode, we first synthesized and characterized 12 manganese oxides with different crystal structures, morphologies, and/or particle sizes (Table S1). Eight of the manganese oxides produced powder X-ray diffraction patterns consistent with a single manganese oxide phase in the International Centre for Diffraction Data (ICDD) database (Figure S3). Three of the manganese oxides produced powder X-ray diffraction patterns that only contained two very broad peaks at approximately the 16° and 29° 2θ (Mo Kα; Figure S3i−k), consistent with published patterns for δ-MnO_2.[35,38,45] We will refer to these three oxides as δ-MnO_2, as opposed to birnessite, because they lacked the characteristic sharp peaks at 5.7° and 11.4° 2θ (Mo Kα; 7.28 and 3.64 Å).[38] The last oxide showed X-ray diffraction peaks consistent with the presence of both ramsdellite (1 × 2 tunnel structure) and pyrolusite (1 × 1 tunnel structure; β-MnO_2; Figure S3d). In prior work using the same synthesis method, the authors also observed these two phases in the powder X-ray diffraction pattern and described the mixture as γ-MnO_2.[36,46] We included the biphasic γ-MnO_2 in our study, despite it being a mixture, because it was previously shown to successfully intercalate cations in an energy storage cell.[46] All 12 manganese oxides were used for subsequent experiments.

The morphologies for the manganese oxides differed, as evidenced by SEM and TEM images (Figure S4). Scanning electron micrographs showed that β-MnO_2-1, β-MnO_2-2, γ-MnO_2, α-MnO_2, and sodium manganese oxide (NMO) consisted of needle or rod-like crystals (Figure S4a,c,d,h,k,aa); Mn_2O_3 and δ-MnO_2-3 consisted of spherical crystals (Figure S4f,g,x,y); hexagonal birnessite and triclinic sodium birnessite consisted of ribbon or flower-like crystals (Figure S4p,n,o,q);

https://dx.doi.org/10.1021/acs.est.0c00096
Environ. Sci. Technol. 2020, 54, 5746−5754

potassium birnessite, δ-MnO_2-1, and δ-MnO_2-2 had large, irregular crystals (Figure S4l,s,u,v). Cross-sectional TEM revealed that potassium birnessite, triclinic sodium birnessite, and hexagonal birnessite had layered structures (Figure S4m,o,r), consistent with the presence of a sharp peak at 7° 2θ (Mo Kα) [001 face] in the X-ray diffraction patterns.[38] For these three oxides, the stacks appeared to be curved, suggesting some disorder.[38] TEM images of δ-MnO_2-1, δ-MnO_2-2, and δ-MnO_2-3 showed nanocrystalline (5−20 nm) particles containing regions that appeared to be stacked layers and regions with amorphous particles (Figure S4t,w,z). δ-MnO_2-1 had larger crystals and more stacking than δ-MnO_2-2 and δ-MnO_2-3, which likely explained its lower BET specific surface area (155 m^2/g) relative to the other two oxides (217 and 314 m^2/g).

Electrical Power Production from a NaCl Salinity Gradient. To compare the electrical power density that each manganese oxide could produce, we fabricated composite manganese oxide electrodes and tested them in a symmetrical, dual-channel concentration flow cell (Figure 2a). We used this cell design because the design was previously shown to generate the highest electrical power densities when harvesting salinity gradient energy using electrode-based reactions.[13−15] The cell contained two identical manganese oxide composite electrodes that were exposed to two waters with different sodium chloride concentrations (30 g/L, 0.5 M and 1 g/L, 0.02 M) flowing at 15 mL/min (hydraulic retention time = 0.14 s). The two flow channels were separated by an anion exchange membrane. Electricity was produced by alternating the water flow paths over each electrode in a two-stage process.

When the electrical circuit was closed with a constant external resistance (see Figure S5 for an explanation for how the resistance was chosen), the cell produced electricity (Figure 2b contains an example data set for δ-MnO_2-2). In the first stage of operation, electrical power initially peaked after a few seconds and then gradually decayed as the cell discharged. The decrease in power production over time was coupled to a decrease in the cell voltage, as explained below. When the cell voltage discharged to a predetermined cutoff voltage (±30 mV), the solution flow paths were switched, resuming electrical power generation (Figure 2b, Stage 2). The cutoff voltage value was based on previous work in our lab that examined its effect on observed peak and average power densities.[13] We could continue to produce electricity over multiple cycles by periodically switching the flow paths of the sodium chloride solutions, consistent with previous studies using the same cell architecture with different electrode materials.[13,14]

The cell voltage (ΔV_{cell}, V) was discharged as electricity via two complementary mechanisms.[13−16,47,48] The first mechanism involved the manganese oxide electrodes. Manganese oxides may develop electrode potentials (E, V) on the basis of the activity of sodium ions in the solution via (pseudo)-capacitive and intercalation reactions, in which Na^+ uptake is coupled to the reduction of Mn^{4+} to Mn^{3+} and generally written as

$$MnO_{2(s)} + Na^+_{(aq)} + e^- \rightleftharpoons MnOONa_{(s)} \quad (3)$$

The actual half-reaction for each manganese oxide depends on its molecular formula. Since each of the two manganese oxide electrodes develop a potential based on the activity of Na^+ in solution, the contribution of this mechanism on the cell voltage ($\Delta V_{electrodes}$) can be written as

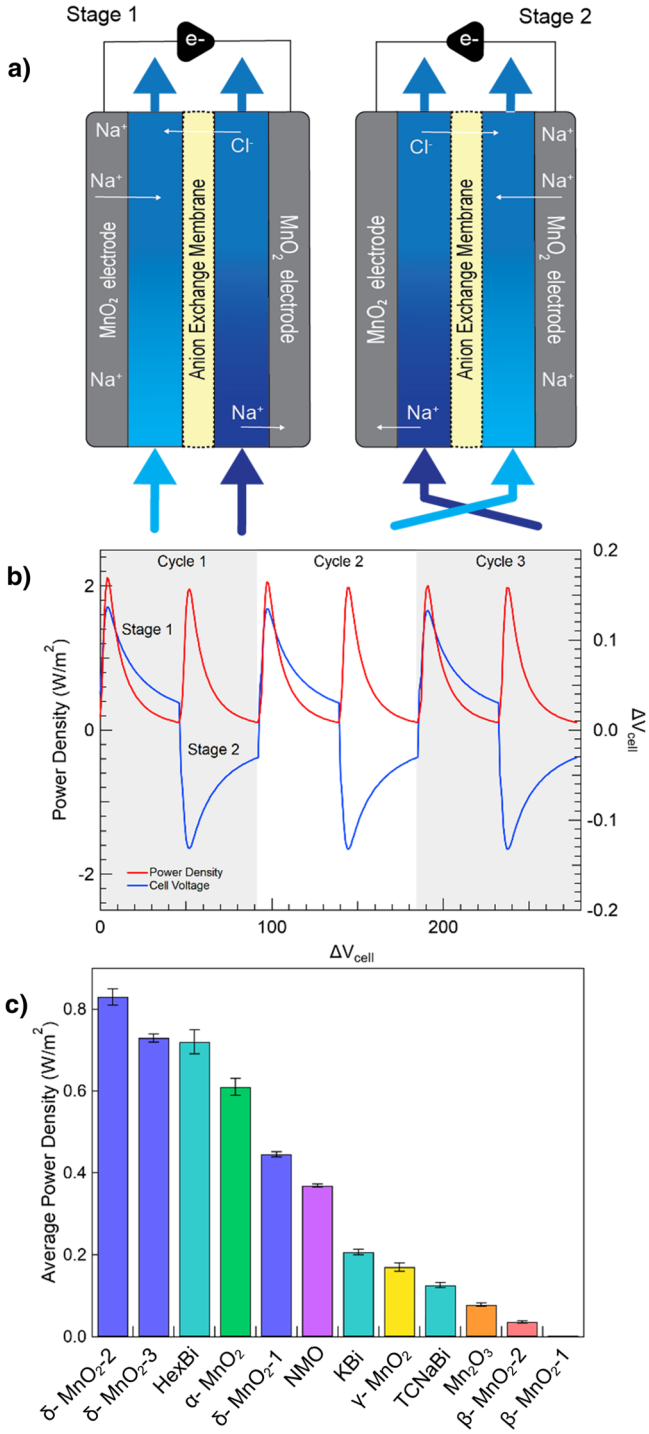

Figure 2. (a) Schematic of the salinity gradient energy flow cell (cell dimensions listed in Figure S2). Energy is produced from the uptake/release of Na^+ by the manganese oxide electrodes and transport of Cl^- through the anion exchange membrane. (b) Representative power density (red curve) and cell voltage (blue curve) profiles generated over three cycles of flow cell operation using δ-MnO_2-2. (c) Measured average power density for manganese oxide electrodes operating in the concentration flow cell using 1 and 30 g/L NaCl solutions at a flow rate of 15 mL/min. Error bars represent standard deviation between cycles.

$$\Delta V_{electrodes} = \frac{RT}{F} \ln\left(\frac{\{Na^+\}_{high\ concentration}}{\{Na^+\}_{low\ concentration}}\right) \quad (4)$$

https://dx.doi.org/10.1021/acs.est.0c00096
Environ. Sci. Technol. 2020, 54, 5746−5754

where R is the gas constant [8.314 J/(mol·K)], T is absolute temperature (298 K in our experiments), and F is Faraday's constant (96 485 C/mol). High concentration refers to the 0.5 M NaCl solution, and low concentration refers to the 0.02 M NaCl solution. Using eq 4, we calculated the theoretical $\Delta V_{electrodes}$ value in the cell to be 0.080 V. The calculated activities of Na^+ and Cl^- were 0.34 for the 0.5 M solution and 0.015 for the 0.02 M solution (Davies model, Visual MINTEQ ver. 3.0).

The second mechanism that contributed to the cell voltage was a Donnan potential that developed across the anion exchange membrane due to the Cl^- activity gradient between the two waters. This voltage (ΔV_{Donnan}) can be described with the following Nernst equation:[13]

$$\Delta V_{Donnan} = \frac{RT}{F} \ln\left(\frac{\{Cl^-\}_{high\ concentration}}{\{Cl^-\}_{low\ concentration}}\right) \quad (5)$$

Using eq 5, we calculated the theoretical ΔV_{Donnan} to be 0.080 V (Davies model, Visual MINTEQ ver. 3.0). The combined contributions of ΔV_{Donnan} and $\Delta V_{electrodes}$ yielded a theoretical ΔV_{cell} value of 0.160 V for all the manganese oxides, which was close to the experimentally measured open-circuit voltage measured for δ-MnO_2-1, δ-MnO_2-2, δ-MnO_2-3, hexagonal birnessite, and sodium manganese oxide (0.15 V, Figure S6). The remaining manganese oxide samples produced cell voltages below the theoretical value; ΔV_{cell} was 0.14 V for α-MnO_2, potassium birnessite, and triclinic sodium birnessite and 0.11 V for β-MnO_2, Mn_2O_3, and γ-MnO_2.

Despite the manganese oxide electrodes having identical theoretical ΔV_{cell} values, the average (and peak) power densities produced by each electrode varied substantially (Figure 2c, Table S1). Note that the external resistance used to collect the highest average power density for each material varied (10−70 Ω; see Table S1 for the external resistances used and Figure S5 for a description of how the external resistance was chosen). The highest average power density is achieved when the external resistance is equal to the internal resistance of the entire cell.[9,49] Also note that we examined how the initial potential of the manganese oxide influenced power production, as described in the following section. The average power density values were calculated by taking the mean power density over the entirety of six stages. The highest average power density detected was 1.18 ± 0.01 W/m^2 using sodium manganese oxide. β-MnO_2-1 produced no appreciable power density because the cell voltage never exceeded the ±30 mV voltage cutoff limit. We showed that the manganese oxide was necessary for power production by using a control cell containing composite electrodes that contained no manganese oxide (data not shown) and did not generate any power. These measured average power densities are consistent with other recent studies (0.015 to 3.8 W/m^2)[12,13,16,50] that used a similar cell architecture but different electrode materials and sodium chloride concentrations.

Relationship of Power Density to Charge Storage Capacity. To understand why the manganese oxide electrodes produced such markedly different power densities, we investigated relationships among the manganese oxides' average power densities and charge storage capacities. We first examined whether the variations in average power densities could be explained by the differences in charge storage capacities. We measured the charge storage capacities of each manganese oxide by integrating cyclic voltammograms of the electrodes when using a scan rate (ν) of 5 mV/s in 1 M NaCl solutions. We used this scan rate because 5 mV/s was approximately equal to the rate at which ΔV_{cell} changed during power production from salinity gradients for the majority of materials tested (i.e., the slope of ΔV_{cell} with respect to time in Figure 2b). The same mass of manganese oxide was present on each electrode (15 ± 3 mg) to facilitate direct comparisons. Overall, we expected that materials with larger charge storage capacities would produce higher power densities because they would be more resilient to voltage changes for the same amount of charge passed through the cell. We also anticipated some deviations from this trend, as cyclic voltammograms were collected over much wider potential windows (0.6 V) than the potential window over which the manganese oxide varied during power generation (~0.16 V).

We observed a positive linear correlation between average power density and charge storage capacity (Figure 3; r^2 = 0.87;

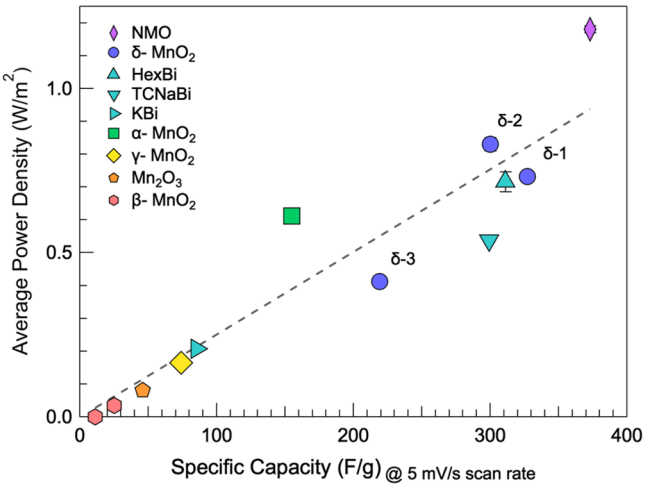

Figure 3. Average power density produced in the flow cell plotted as a function of specific capacity for each manganese oxide sample. Specific capacities were calculated from CVs performed in a 3-electrode cubic cell in 1 M NaCl at a 5 mV/s scan rate. The linear regression for a sample set without outliers is shown (gray dotted line); slope = 0.00244 ± 0.00016. Error bars are contained within the markers for some data points.

power density [W/m^2] = 0.0025 ± 0.00017(σ) × capacity [F/g]; the regression was forced through the origin), indicating that manganese oxides with higher capacities generally produced higher power densities. A similar positive correlation was seen between peak power density and charge storage capacity (data not shown). Among the cyclic voltammograms for the 12 manganese oxides, 10 materials exhibited rectangular cyclic voltammograms indicative of (pseudo)capacitive charging (Figure 4). Two materials, triclinic sodium birnessite and sodium manganese oxide, differed in that they both contained distinct peaks, indicative of intercalation reactions (Figure 4g,l). The strong linear trend between average power density and charge storage capacity indicated that charge storage capacity measurements may be a relatively simple way to screen potential electrode materials for harvesting sodium chloride-based salinity gradient energy.

We examined if the initial potential of the manganese oxide influenced electrical power production considering that two of the materials (sodium manganese oxide and triclinic sodium birnessite) showed peaks in their CVs clearly indicative of

https://dx.doi.org/10.1021/acs.est.0c00096
Environ. Sci. Technol. 2020, 54, 5746−5754

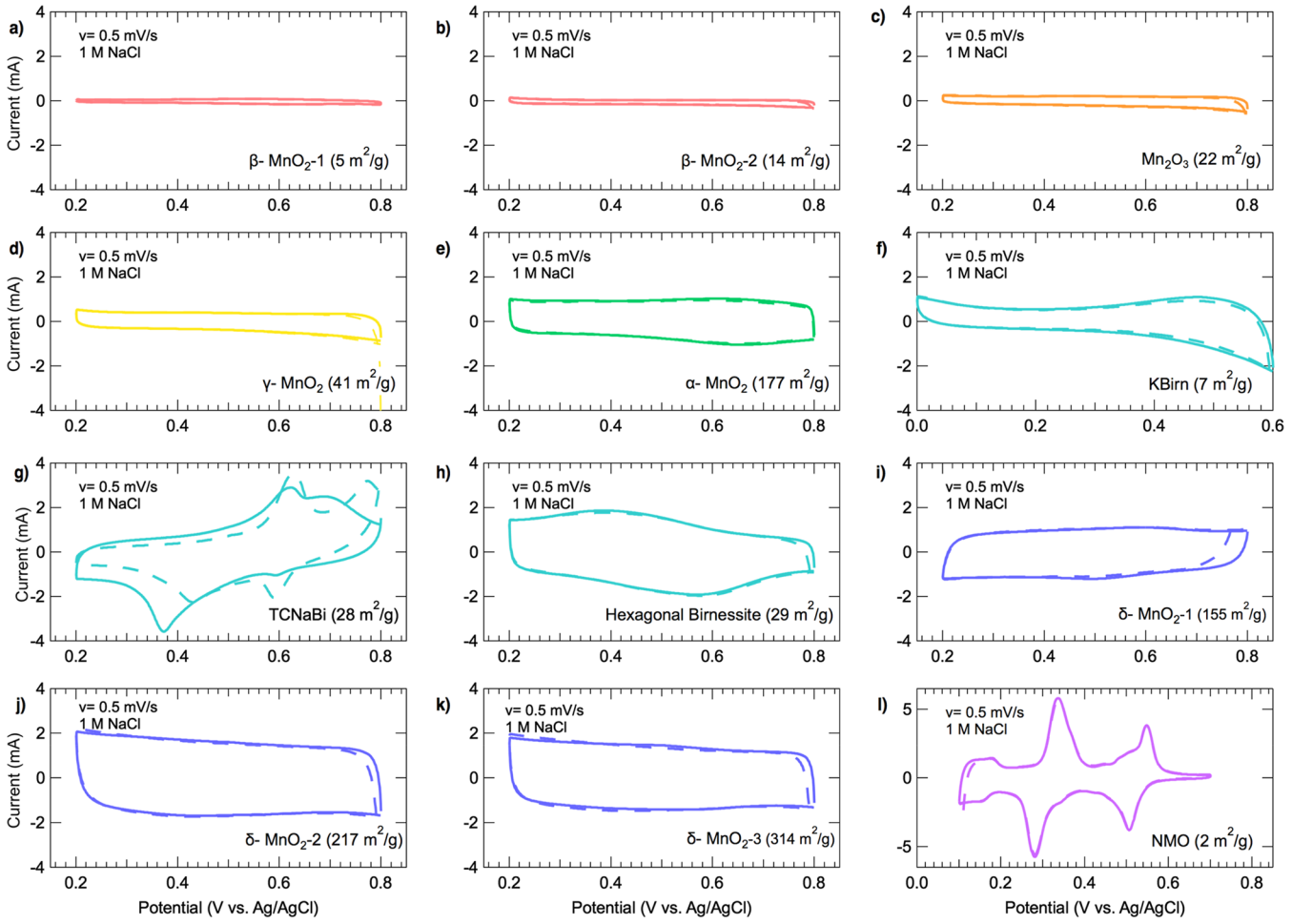

Figure 4. Cyclic voltammetry scans (0.5 mV/s, 1 M NaCl electrolyte) for each manganese oxide sample. CVs were performed in 3-electrode cubic cells with a Ag/AgCl reference electrode and Pt counter electrode. Three cyclic sweeps were performed for each material; the first sweep (dotted line) and third sweep (solid line) are reported here.

intercalation reactions. For these two materials, power densities varied depending on their initial potential (Figure S7). The power densities they produced were the highest for these materials when the potential was poised to a value near the midpoint potential for peaks in the cyclic voltammograms. For manganese oxides that exhibited rectangular, (pseudo)-capacitive cyclic voltammograms, we did not observe changes in power production after the electrodes were poised at potentials within the stable potential window (0.2−0.8 V vs Ag/AgCl; data not shown). The power densities provided in Figure 2 and used in the subsequent figures represent the highest electrical power densities we achieved for each material as a function of initial potential.

Role of Manganese Oxide Specific Surface Areas. The correlation between average power density and charge storage capacity led us to investigate why the manganese oxides exhibited such a wide range of charge storage capacities. We first examined how manganese oxide charge storage capacities related to specific surface areas. Plotting charge storage capacity (υ = 5 mV/s, 1 M NaCl) against BET specific surface area values yielded a strong positive correlation when four outliers were removed: potassium birnessite, triclinic sodium birnessite, hexagonal birnessite, and sodium manganese oxide (Figure 5; r^2 = 0.92, n = 8; power density [W/m^2] = 1.1492 ± 0.0793 × capacity [F/g]; the regression was forced through the origin). The positive correlation between charge storage

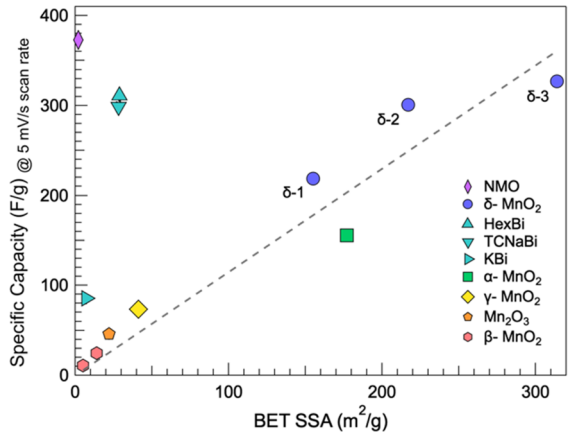

Figure 5. For each manganese oxide sample, we compared specific capacity (from CVs at a 5 mV/s scan rate in 1 M NaCl) as a function of BET specific surface area (SSA). The linear regression for the sample set without outliers is shown (gray dotted line); slope = 1.1492 ± 0.0793. Error bars are contained within the markers for some data points.

capacity and BET specific surface area suggested that a considerable amount of the capacities for eight of the materials (i.e., not the outliers) was attributable to (pseudo)capacitive reactions at their surfaces. This trend is consistent with past

https://dx.doi.org/10.1021/acs.est.0c00096
Environ. Sci. Technol. 2020, 54, 5746−5754

studies demonstrating that manganese oxide charge storage capacities positively correlate with BET specific surface area values.[21,32] The four outliers exhibited higher ratios of charge storage capacities to BET specific surface area values than the other eight manganese oxides (Figure 5). The most likely explanation for this observation is that these oxides charged predominately through intercalation mechanisms. To determine if this was the case, we performed additional experiments in which we examined cyclic voltammograms over a series of scan rates for each oxide.

Charge Storage Analysis of Manganese Oxide Electrodes. We collected cyclic voltammograms for each oxide as a function of scan rate (v = 0.1−50 mV/s) in 1 M NaCl over a potential window of 0.2 to 0.8 V vs Ag/AgCl. The manganese oxides' charge storage capacities, which were calculated by integrating cyclic voltammograms, were larger at lower scan rates and in the more concentrated NaCl solution (Figure S8).[22,29,51] We examined the peak current (I_{peak}) value in the cathodic and anodic scans as a function of v to estimate the relative contributions of (pseudo)capacitive surface reaction ($I_{peak} \propto v$) and diffusion-controlled intercalation reaction ($I_{peak} \propto v^{1/2}$) processes.[22,51,52] We initially estimated the relative contributions of these two mechanisms by approximating the b value (eq 3), with b = 1 indicating a purely (pseudo)capacitive process, b = 0.5 indicating a purely diffusion-controlled intercalation process, and 0.5 < b < 1 indicating a combination of the two.[22] In 1 M NaCl, the b values for the manganese oxides range from 0.60 (sodium manganese oxide) to 0.92 (α-MnO_2), indicating that the relative contributions of (pseudo)capacitive and intercalation reactions differed substantially among the oxides (Table 1). We used these data to test our hypothesis that the four outliers in Figure 5 charged predominately through intercalation mechanisms.

Table 1. Charge Storage Analysis for Manganese Oxide Electrodes[a]

Manganese oxide	Average *b*-value
β-MnO_2-1	0.85 ± 0.07
β-MnO_2-2	0.83 ± 0.05
Mn_2O_3	0.86 ± 0.02
γ-MnO_2	0.82 ± 0.02
α-MnO_2	0.92 ± 0.04
K Birnessite	0.62 ± 0.08
TC Na Birnessite	0.74 ± 0.09
Hex Birnessite	0.90 ± 0.01
δ-MnO_2-1	0.90 ± 0.02
δ-MnO_2-2	0.90 ± 0.04
δ-MnO_2-3	0.90 ± 0.10
NMO	0.60 ± 0.02

[a]The b value reports on surface vs diffusion-controlled current response (capacitive response, b = 1; diffusion-controlled response, b = 0.5).

Three of these four manganese oxides exhibited the lowest b values (sodium manganese oxide: 0.60 ± 0.02; potassium birnessite: 0.62 ± 0.08; triclinic sodium birnessite: 0.74 ± 0.09), consistent with our hypothesis. The final outlier, hexagonal birnessite, did not fit the trend, however, as the b value was much higher (0.90 ± 0.01). We suspect the reason why that hexagonal birnessite exhibited such a high specific charge storage capacity relative to the BET specific surface area is that the BET measurements contained an artifact, despite being measured twice (specific surface area (SSA) = 29.0 ± 0.2, n = 2 measurements). This SSA was surprisingly low given that TEM images indicated nanoparticulate 5−10 nm flower-like particles (Figure S4q). One reason the BET measurements may have yielded an inaccurate specific surface area value was that the hexagonal birnessite may have contained Na^+, which has been shown to influence BET measurements.[28,38]

On the basis of the b analysis, the remaining eight manganese oxides charged predominately through surface (pseudo)capacitive reactions (b values range from 0.82 to 0.90, Table S2). This indicates that, even though many of these oxides could potentially intercalate Na^+ into tunnels or interlayers (Figure 1), those processes only contributed a small fraction (<20%) to their overall capacities under the conditions tested. Overall, these analyses supported our conclusion that power production correlates with specific capacity, and intercalation reactions can enhance material performance by increasing charge storage capabilities, regardless of surface area.

Implications for Power Generation from Salinity Gradients. Our results collectively indicate that power production from NaCl salinity gradients using manganese oxide electrodes can occur via (pseudo)capacitive reactions at manganese oxide surfaces or intercalation reactions (if the material is capable of intercalation). For the 12 manganese oxides surveyed, there was a strong linear correlation between the average electrical power density they produced when harvesting salinity gradient energy and their specific capacities recorded from cyclic voltammograms collected at a scan rate similar to the change in voltage observed when harvesting salinity gradient energy (i.e., 5 mV/s). This linear correlation suggests that cyclic voltammetry may be a simple means for screening potential materials for harvesting salinity gradient energy.

The data also demonstrate that manganese oxides capable of intercalation yield higher electrical power densities than those that rely solely on (pseudo)capacitive reactions. We found that, in order to maximize the electrical power densities of manganese oxide electrodes capable of intercalation, the electrodes must first be poised to a potential near the effective reduction potential of the intercalation reaction. This finding is particularly important given that the potentials of the intercalating electrode materials were not prepoised prior to harvesting salinity gradient energy in past studies,[9−11,13,14,53] and therefore, prepoising electrodes may also improve the performance of previously studied materials that exhibit distinct intercalating peaks in cyclic voltammograms. For the manganese oxides that produced electricity primarily through surface (pseudo)capacitive reactions, electrical power densities strongly correlated with BET specific surface area values and specific capacitance values, indicating that (pseudo)capacitive materials could be improved by maximizing their specific surface area values, a trend that can be applied to other active materials that rely predominantly on surface reactions.

■ ASSOCIATED CONTENT

Supporting Information

The Supporting Information is available free of charge at https://pubs.acs.org/doi/10.1021/acs.est.0c00096.

https://dx.doi.org/10.1021/acs.est.0c00096
Environ. Sci. Technol. 2020, 54, 5746−5754

Manganese oxide syntheses; image of 3-electrode electrochemical cell; image of concentration flow cell; data for BET surface area, capacity measurements, and power density measurements; powder X-ray diffraction patterns; SEM and TEM images; representative average power density curve in the concentration flow cell; representative open-circuit voltage curve in the concentration flow cell; power density as a function of initial potential of manganese oxide electrode; specific capacity measurements as a function of scan rate and NaCl concentration (PDF)

AUTHOR INFORMATION

Corresponding Author

Christopher A. Gorski − *Department of Civil and Environmental Engineering, The Pennsylvania State University, University Park, Pennsylvania 16802, United States;* orcid.org/0000-0002-5363-2904; Phone: +1-814-865-5673; Email: cag981@psu.edu

Authors

Jenelle Fortunato − *Department of Civil and Environmental Engineering, The Pennsylvania State University, University Park, Pennsylvania 16802, United States*

Jasquelin Peña − *Institute of Earth Surface Dynamics, University of Lausanne, CH-1015 Lausanne, Switzerland;* orcid.org/0000-0001-7081-3873

Sassi Benkaddour − *Institute of Earth Surface Dynamics, University of Lausanne, CH-1015 Lausanne, Switzerland;* orcid.org/0000-0003-1583-4211

Huichun Zhang − *Department of Civil Engineering, Case Western Reserve University, Cleveland, Ohio 44106, United States;* orcid.org/0000-0002-5683-5117

Jianzhi Huang − *Department of Civil Engineering, Case Western Reserve University, Cleveland, Ohio 44106, United States*

Mengqiang Zhu − *Department of Ecosystem Science and Management, University of Wyoming, Laramie, Wyoming 82071, United States;* orcid.org/0000-0003-1739-1055

Bruce E. Logan − *Department of Civil and Environmental Engineering, The Pennsylvania State University, University Park, Pennsylvania 16802, United States;* orcid.org/0000-0001-7478-8070

Complete contact information is available at: https://pubs.acs.org/10.1021/acs.est.0c00096

Notes

The authors declare no competing financial interest.

ACKNOWLEDGMENTS

This research was supported by the National Science Foundation (CBET-1603635) and an internal seed grant from the Pennsylvania State University. J.P. acknowledges support from the Swiss National Science Foundation (Project 200020_162825). Material characterization was made possible by the instrumentation and technical support provided at the Penn State Materials Characterization Lab. We thank Dr. Taeyoung Kim (Dept. of Chemical and Biomolecular Engineering, Clarkson University) for his mentorship to J.F.

REFERENCES

(1) Li, W.; Krantz, W. B.; Cornelissen, E. R.; Post, J. W.; Verliefde, A. R. D.; Tang, C. Y. A Novel Hybrid Process of Reverse Electrodialysis and Reverse Osmosis for Low Energy Seawater Desalination and Brine Management. *Appl. Energy* **2013**, *104*, 592−602.

(2) Yip, N. Y.; Brogioli, D.; Hamelers, H. V. M.; Nijmeijer, K. Salinity Gradients for Sustainable Energy: Primer, Progress, and Prospects. *Environ. Sci. Technol.* **2016**, *50*, 12072−12094.

(3) Logan, B. E.; Elimelech, M. Membrane-Based Processes for Sustainable Power Generation Using Water. *Nature* **2012**, *488* (7411), 313−319.

(4) Tufa, R. A.; Pawlowski, S.; Veerman, J.; Bouzek, K.; Fontananova, E.; di Profio, G.; Velizarov, S.; Goulão Crespo, J.; Nijmeijer, K.; Curcio, E. Progress and Prospects in Reverse Electrodialysis for Salinity Gradient Energy Conversion and Storage. *Appl. Energy* **2018**, *225* (March), 290−331.

(5) Gerstandt, K.; Peinemann, K. V.; Skilhagen, S. E.; Thorsen, T.; Holt, T. Membrane Processes in Energy Supply for an Osmotic Power Plant. *Desalination* **2008**, *224* (1−3), 64−70.

(6) Wan, C. F.; Chung, T. S. Osmotic Power Generation by Pressure Retarded Osmosis Using Seawater Brine as the Draw Solution and Wastewater Retentate as the Feed. *J. Membr. Sci.* **2015**, *479*, 148−158.

(7) Yip, N. Y.; Elimelech, M. Thermodynamic and Energy Efficiency Analysis of Power Generation from Natural Salinity Gradients by Pressure Retarded Osmosis. *Environ. Sci. Technol.* **2012**, *46* (9), 5230−5239.

(8) Brogioli, D.; Ziano, R.; Rica, R. A.; Salerno, D.; Kozynchenko, O.; Hamelers, H. V. M.; Mantegazza, F. Exploiting the Spontaneous Potential of the Electrodes Used in the Capacitive Mixing Technique for the Extraction of Energy from Salinity Difference. *Energy Environ. Sci.* **2012**, *5* (12), 9870−9880.

(9) Kim, T.; Rahimi, M.; Logan, B. E.; Gorski, C. A. Harvesting Energy from Salinity Differences Using Battery Electrodes in a Concentration Flow Cell. *Environ. Sci. Technol.* **2016**, *50* (17), 9791−9797.

(10) La Mantia, F.; Pasta, M.; Deshazer, H. D.; Logan, B. E.; Cui, Y. Water Salinity Difference. *Nano Lett.* **2011**, *11*, 1810−1813.

(11) Lee, J.; Yoon, H.; Lee, J.; Kim, T.; Yoon, J. Extraction of Salinity-Gradient Energy by a Hybrid Capacitive-Mixing System. *ChemSusChem* **2017**, *10* (7), 1600−1606.

(12) Kim, T.; Rahimi, M.; Logan, B. E.; Gorski, C. A. Evaluating Battery-like Reactions to Harvest Energy from Salinity Differences Using Ammonium Bicarbonate Salt Solutions. *ChemSusChem* **2016**, *9* (9), 981−988.

(13) Kim, T.; Logan, B. E.; Gorski, C. A. High Power Densities Created from Salinity Differences by Combining Electrode and Donnan Potentials in a Concentration Flow Cell. *Energy Environ. Sci.* **2017**, *10* (4), 1003−1012.

(14) Whiddon, E.; Zhu, H.; Zhu, X. Sodium-Ion Concentration Flow Cell Stacks for Salinity Gradient Energy Recovery: Power Generation of Series and Parallel Configurations. *J. Power Sources* **2019**, *435* (July), 226796−226802.

(15) Sales, B. B.; Liu, F.; Schaetzle, O.; Buisman, C. J. N.; Hamelers, H. V. M. Electrochemical Characterization of a Supercapacitor Flow Cell for Power Production from Salinity Gradients. *Electrochim. Acta* **2012**, *86*, 298−304.

(16) Sales, B. B.; Saakes, M.; Post, J. W.; Buisman, C. J. N.; Biesheuvel, P. M.; Hamelers, H. V. M. Direct Power Production from a Water Salinity Difference in a Membrane-Modified Supercapacitor Flow Cell. *Environ. Sci. Technol.* **2010**, *44* (14), 5661−5665.

(17) Hatzell, M. C.; Cusick, R. D.; Logan, B. E. Capacitive Mixing Power Production from Salinity Gradient Energy Enhanced through Exoelectrogen-Generated Ionic Currents. *Energy Environ. Sci.* **2014**, *7* (3), 1159−1165.

(18) Straub, A. P.; Yip, N. Y.; Elimelech, M. Raising the Bar: Increased Hydraulic Pressure Allows Unprecedented High Power Densities in Pressure-Retarded Osmosis. *Environ. Sci. Technol. Lett.* **2014**, *1* (1), 55−59.

(19) Brousse, T.; Belanger, D.; Long, J. W. To Be or Not To Be Pseudocapacitive? *J. Electrochem. Soc.* **2015**, *162* (5), A5185−A5189.

(20) Kuo, S.-L.; Wu, N.-L. Investigation of Pseudocapacitive Charge-Storage Reaction of $MnO_2{\cdot}nH_2O$ Supercapacitors in Aqueous Electrolytes. *J. Electrochem. Soc.* **2006**, *153* (7), A1317.
(21) Toupin, M.; Brousse, T.; Bélanger, D. Influence of Microstucture on the Charge Storage Properties of Chemically Synthesized Manganese Dioxide. *Chem. Mater.* **2002**, *14* (9), 3946−3952.
(22) Wang, J.; Polleux, J.; Lim, J.; Dunn, B. Pseudocapacitive Contributions to Electrochemical Energy Storage in TiO_2 (Anatase) Nanoparticles. *J. Phys. Chem. C* **2007**, *111* (40), 14925−14931.
(23) Post, J. E. Manganese Oxide Minerals : Crystal Structures and Economic And. *Proc. Natl. Acad. Sci. U. S. A.* **1999**, *96* (March), 3447−3454.
(24) Devaraj, S.; Munichandraiah, N. Effect of Crystallographic Structure of MnO_2 on Its Electrochemical Capacitance Properties. *J. Phys. Chem. C* **2008**, *112* (11), 4406−4417.
(25) Musil, M.; Choi, B.; Tsutsumi, A. Morphology and Electrochemical Properties of α-, β-, γ-, and δ-MnO_2 Synthesized by Redox Method. *J. Electrochem. Soc.* **2015**, *162* (10), A2058−A2065.
(26) Feng, Q.; Kanoh, H.; Ooi, K. Manganese Oxide Porous Crystal. *J. Mater. Chem.* **1999**, *9*, 319−333.
(27) Liu, Y.; Wei, J.; Tian, Y.; Yan, S. The Structure−Property Relationship of Manganese Oxides: Highly Efficient Removal of Methyl Orange from Aqueous Solution. *J. Mater. Chem. A* **2015**, *3* (37), 19000−19010.
(28) Marafatto, F. F.; Lanson, B.; Peña, J. Crystal Growth and Aggregation in Suspensions of δ-MnO_2 Nanoparticles: Implications for Surface Reactivity. *Environ. Sci.: Nano* **2018**, *5* (2), 497−508.
(29) Costentin, C.; Porter, T. R.; Savéant, J. M. How Do Pseudocapacitors Store Energy? Theoretical Analysis and Experimental Illustration. *ACS Appl. Mater. Interfaces* **2017**, *9* (10), 8649−8658.
(30) Wei, W.; Cui, X.; Chen, W.; Ivey, D. G. Manganese Oxide-Based Materials as Electrochemical Supercapacitor Electrodes. *Chem. Soc. Rev.* **2011**, *40* (3), 1697−1721.
(31) Toupin, M.; Brousse, T.; Bélanger, D. Charge Storage Mechanism of MnO_2 Electrode Used in Aqueous Electrochemical Capacitor. *Chem. Mater.* **2004**, *16* (16), 3184−3190.
(32) Conway, B. E.; Birss, V.; Wojtowicz, J. The Role and Utilization of Pseudocapacitance for Energy Storage by Supercapacitors. *J. Power Sources* **1997**, *66* (1−2), 1−14.
(33) Julien, C.; Mauger, A. Nanostructured MnO_2 as Electrode Materials for Energy Storage. *Nanomaterials* **2017**, *7* (11), 396.
(34) Brousse, T.; Toupin, M.; Dugas, R.; Athouël, L.; Crosnier, O.; Bélanger, D. Crystalline MnO_2 as Possible Alternatives to Amorphous Compounds in Electrochemical Supercapacitors. *J. Electrochem. Soc.* **2006**, *153* (12), A2171.
(35) McKenzie, R. M. The Synthesis of Birnessite, Cryptomelane, and Some Other Oxides and Hydroxides of Manganese. *Mineral. Mag.* **1971**, *38* (296), 493−502.
(36) de Wolff, P. M. Interpretation of Some γ-MnO_2 Diffraction Patterns. *Acta Crystallogr.* **1959**, *12* (4), 341−345.
(37) Fleischer, M.; Richmond, W. E. The Manganese Oxide Minerals: A Preliminary Report. *Econ. Geol. Bull. Soc. Econ. Geol.* **1943**, *38*, 269.
(38) Zhu, M.; Farrow, C. L.; Post, J. E.; Livi, K. J. T.; Billinge, S. J. L.; Ginder-Vogel, M.; Sparks, D. L. Structural Study of Biotic and Abiotic Poorly-Crystalline Manganese Oxides Using Atomic Pair Distribution Function Analysis. *Geochim. Cosmochim. Acta* **2012**, *81*, 39−55.
(39) Kim, T.; Gorski, C. A.; Logan, B. E. Low Energy Desalination Using Battery Electrode Deionization. *Environ. Sci. Technol. Lett.* **2017**, *4* (10), 444−449.
(40) Liu, T.; Pell, W. G.; Conway, B. E. Self-Discharge and Potential Recovery Phenomena at Thermally and Electrochemically Prepared RuO_2 supercapacitor Electrodes. *Electrochim. Acta* **1997**, *42* (23−24), 3541−3552.
(41) Brezesinski, K.; Wang, J.; Haetge, J.; Reitz, C.; Steinmueller, S. O.; Tolbert, S. H.; Smarsly, B. M.; Dunn, B.; Brezesinski, T. Pseudocapacitive Contributions to Charge Storage in Highly Ordered Mesoporous Group V Transition Metal Oxides with Iso-Oriented Layered Nanocrystalline Domains. *J. Am. Chem. Soc.* **2010**, *132* (20), 6982−6990.
(42) Augustyn, V.; Simon, P.; Dunn, B. Pseudocapacitive Oxide Materials for High-Rate Electrochemical Energy Storage. *Energy Environ. Sci.* **2014**, *7* (5), 1597−1614.
(43) Augustyn, V.; Come, J.; Lowe, M. A.; Kim, J. W.; Taberna, P. L.; Tolbert, S. H.; Abruña, H. D.; Simon, P.; Dunn, B. High-Rate Electrochemical Energy Storage through Li^+ Intercalation Pseudocapacitance. *Nat. Mater.* **2013**, *12* (6), 518−522.
(44) Bard, A. J.; Faulkner, L. R. *Fundamentals and Fundamentals and Applications*; 2015; Vol. *8*.
(45) Villalobos, M.; Bargar, J.; Sposito, G. Trace Metal Retention on Biogenic Manganese Oxide Nanoparticles. *Elements* **2005**, *1* (4), 223−226.
(46) Walanda, D. K.; Lawrance, G. A.; Donne, S. W. Kinetics of Mn_2O_3 digestion in H_2SO_4 solutions. *J. Solid State Chem.* **2009**, *182* (6), 1336−1342.
(47) Liu, F.; Schaetzle, O.; Sales, B. B.; Saakes, M.; Buisman, C. J. N.; Hamelers, H. V. M. Effect of Additional Charging and Current Density on the Performance of Capacitive Energy Extraction Based on Donnan Potential. *Energy Environ. Sci.* **2012**, *5* (9), 8642−8650.
(48) Nakayama, M.; Konishi, S.; Tagashira, H.; Ogura, K. Electrochemical Synthesis of Layered Manganese Oxides Intercalated with Tetraalkylammonium Ions. *Langmuir* **2005**, *21* (1), 354−359.
(49) Cheng, S.; Liu, H.; Logan, B. E. Increased Power Generation in a Continuous Flow MFC with Advective Flow through the Porous Anode and Reduced Electrode Spacing. *Environ. Sci. Technol.* **2006**, *40* (7), 2426−2432.
(50) Marino, M.; Misuri, L.; Ruffo, R.; Brogioli, D. Electrode Kinetics in the "Capacitive Mixing" and "Battery Mixing" Techniques for Energy Production from Salinity Differences. *Electrochim. Acta* **2015**, *176*, 1065−1073.
(51) Patel, M. N.; Wang, X.; Slanac, D. A.; Ferrer, D. A.; Dai, S.; Johnston, K. P.; Stevenson, K. J. High Pseudocapacitance of MnO_2 Nanoparticles in Graphitic Disordered Mesoporous Carbon at High Scan Rates. *J. Mater. Chem.* **2012**, *22* (7), 3160−3169.
(52) Liu, T.-C. Behavior of Molybdenum Nitrides as Materials for Electrochemical Capacitors. *J. Electrochem. Soc.* **1998**, *145* (6), 1882.
(53) Zhu, X.; Xu, W.; Tan, G.; Wang, Y. Concentration Flow Cells for Efficient Salinity Gradient Energy Recovery with Nanostructured Open Framework Hexacyanoferrate Electrodes. *ChemistrySelect* **2018**, *3* (20), 5571−5580.

https://dx.doi.org/10.1021/acs.est.0c00096
Environ. Sci. Technol. 2020, 54, 5746−5754